

**New Production Rate Estimates for In Situ Cosmogenic  $^{14}\text{C}$  from Lake Bonneville, Utah,  
and Northwestern Scotland**

**by**

**Bailey Dugan**

**A Prepublication Manuscript Submitted to the Faculty of the**

**DEPARTMENT OF GEOSCIENCES**

**In Partial Fulfillment of the Requirements for the Degree of**

**MASTER OF SCIENCE**

**In the Graduate College  
THE UNIVERSITY OF ARIZONA  
2008**



**New Production Rate Estimates for In Situ Cosmogenic  $^{14}\text{C}$  from Lake Bonneville, Utah,  
and Northwestern Scotland**

Bailey Dugan<sup>1\*</sup>, Nathaniel A. Lifton<sup>1</sup>, A.J. Timothy Jull<sup>1</sup>

(1) Geosciences Department and Arizona AMS Facility, University of Arizona, Tucson, AZ  
85721, U.S.A.

\* Corresponding author: [bdugan23@hotmail.com](mailto:bdugan23@hotmail.com)

**Abstract**

Terrestrial in situ cosmogenic nuclide (TCN) analytical techniques have enabled broad advances in Quaternary geologic and surficial process research over the past two decades. However, the lack of a commonly accepted framework for TCN measurements and spatial and temporal production rate scaling has limited the ability to draw robust comparisons on a global scale. The CRONUS-Earth Project and CRONUS-EU seek to remedy this situation through a multidisciplinary investigation of TCN production and measurement systematics.

Under the CRONUS-Earth Project, we aim to improve the calibration of in situ cosmogenic  $^{14}\text{C}$  (in situ  $^{14}\text{C}$ ) production rates. In situ  $^{14}\text{C}$  is a particularly useful nuclide for late Quaternary surficial process studies by virtue of its short half-life (5730 y) – unique among commonly measured TCNs. However, current estimates of in situ  $^{14}\text{C}$  production rates are based primarily on replicate measurements of a single sample from one calibration site associated with Pleistocene Lake Bonneville in Utah. A more robust approach would be to measure TCN production rates from multiple samples at multiple sites with well-constrained exposure histories, covering as wide a spatial and temporal range as possible. This is the approach taken by the CRONUS-Earth Project.

Here we present new in situ  $^{14}\text{C}$  production rate estimates based on analyses of multiple samples from two calibration sites. The first site is on a wave-cut shoreline associated with Pleistocene Lake Bonneville at Promontory Point, Utah, while late-Glacial age landforms in the Highlands of northwestern Scotland comprise the second site. We use extraction techniques based on those of Lifton et al. (2001. A new extraction technique and production rate estimate for in situ cosmogenic  $^{14}\text{C}$  in quartz. *Geochimica et Cosmochimica Acta*. 65, 1953-1969) and Pigati (2004. Experimental developments and application of carbon-14 and in situ cosmogenic

nuclide dating techniques. Ph.D. Thesis, University of Arizona, Tucson.), along with more vigorous pretreatment procedures, to ensure accurate measurement of in situ  $^{14}\text{C}$  nuclide concentrations. We argue that these techniques, combined with careful calibration site and sample selection, result in production rate estimates for in situ  $^{14}\text{C}$  that are more robust than previously published values. We also scale our results to sea level and high latitude, using published scaling models, to compare estimates of reference in situ  $^{14}\text{C}$  production rates.

**Keywords:** terrestrial cosmogenic nuclides, production rates, in situ  $^{14}\text{C}$ , Lake Bonneville, Scotland

## 1. Introduction

Terrestrial in situ cosmogenic nuclide (TCN) analytical techniques have enabled broad advances in Quaternary geologic and surficial process research over the past two decades. However, the lack of a commonly accepted framework for TCN measurements and spatial and temporal production rate scaling has limited the ability to draw robust comparisons on a global scale. As techniques for interpreting TCN data advance, they often require higher precision and accuracy than the typical current estimates of ~10% to 20% ( $1\sigma$ ) (Gosse and Phillips, 2001). To address this situation, the CRONUS-Earth (Cosmic-Ray Produced Nuclide Systematics on Earth) (<http://www.physics.purdue.edu/primelab/CronusProject/cronus/>) and CRONUS-EU (Cosmic-Ray Produced Nuclide Systematics – The European Contribution) (<http://www.cronus-eu.net/>) Projects were undertaken in North America and Europe, respectively. The collaborating projects intend to place TCN research on an internally consistent foundation, and aim to reduce overall uncertainties to ~5% ( $1\sigma$ ), regardless of location or time frame.

A specific objective of the CRONUS-Earth Project is to improve the quality of TCN production rate estimates, as accurate estimates are critical to many TCN applications. Most existing production rate estimates have been derived from measured nuclide concentrations in independently dated, well-preserved rock surfaces. These “calibrated” estimates are typically converted to reference production rates by scaling them to sea-level and high geomagnetic latitude ( $>60^\circ$ , where the cosmic-ray flux is insensitive to geomagnetic variations). Scaled rates can then be combined to yield an overall modern (if time-dependent effects are accounted for), or time-integrated (if time-dependent effects are neglected), reference production rate estimate for each nuclide. Current reference production rates generally utilize calibrated estimates from a limited range of latitude, altitude, and exposure durations, and thus may be biased. The

CRONUS-Earth Project seeks to improve these estimates by utilizing only the highest quality calibration sites with the most geographic and temporal range possible. It also aims to maximize the number of nuclides that can be measured at each site to ensure directly comparable calibrations, while simultaneously testing the applicability of altitude-latitude scaling factors for commonly measured TCNs.

Under the CRONUS-Earth Project, we aim to improve the calibration of in situ cosmogenic  $^{14}\text{C}$  (in situ  $^{14}\text{C}$ ) production rates. In situ  $^{14}\text{C}$  is particularly useful for late Quaternary surficial process studies by virtue of its short half-life (5.73 ky) – unique among commonly measured TCNs. However, in situ  $^{14}\text{C}$  has not seen common use, as reliable extraction methods are both time- and labor-intensive (Lifton et al., 2001; Pigati, 2004). Current estimates of in situ  $^{14}\text{C}$  production rates are based primarily on replicate measurements of a single sample from one calibration site associated with Pleistocene Lake Bonneville in Utah (Lifton et al., 2001). While Lifton et al. (2001) and subsequent analyses presented in Miller et al. (2006) achieved good reproducibility from this sample, questions regarding sample-to-sample variability at a given site and among multiple sites have not been thoroughly addressed. Here, we report new in situ  $^{14}\text{C}$  production rate estimates based on analyses of multiple samples from the first two CRONUS-Earth calibration sites: shoreline features associated with Pleistocene Lake Bonneville, Utah, and late-Glacial age landforms in the Highlands of northwestern Scotland. Analyses of samples from additional CRONUS-Earth calibration sites are in progress and will be presented in future publications.

Below, we summarize basic production rate systematics, describe the calibration sites and the criteria used for sample selection, and briefly describe laboratory methods. We then present and discuss the in situ  $^{14}\text{C}$  measurements and calculate site-specific in situ  $^{14}\text{C}$  production rates.

Finally, we compare in situ  $^{14}\text{C}$  production rates scaled to sea level and high latitude using four currently published scaling models.

## 2. Production Rate Systematics

The concentration of a radioactive TCN in an exposed surface, as a function of depth below the ground surface ( $z$ , in cm) and exposure time ( $t$ , in y), is described by

$$\frac{dC(z,t)}{dt} = -\lambda C(z,t) + P(z,t) \quad (1)$$

where  $C(z, t)$  is the measured nuclide concentration in atoms  $\text{g}^{-1}$ ,  $P(z, t)$  is the nuclide production rate in atoms  $\text{g}^{-1} \text{y}^{-1}$ , and  $\lambda$  is the radioactive decay constant  $((\ln 2)/t_{1/2})$  (Lal, 1991).

Assuming a constant cosmic ray flux and negligible erosion, the solution to (1) in terms of  $P_0$  (the nuclide production rate at the ground surface), yields

$$C(z,t) = C_0(z,t)e^{-\lambda t} + \frac{P_0 e^{-z\rho/\Lambda}}{\lambda} (1 - e^{-\lambda t}) \quad (2)$$

where  $C_0$  is the radionuclide concentration inherited from a prior exposure history,  $\rho$  is the rock or sediment density, and  $\Lambda$  is the effective attenuation length in terrestrial materials for production of a given TCN (the distance over which TCN production decreases by a factor of e). If nuclide inheritance can be neglected, (2) can be solved for  $P_0$ , yielding

$$P_0 = \frac{C\lambda e^{z\rho/\Lambda}}{1 - e^{-\lambda t}} \quad (3)$$

Since the sites and samples used by CRONUS-Earth for the calibration of TCN production rates were carefully chosen to ensure that inheritance and erosion were negligible, we use (3) for our in situ  $^{14}\text{C}$  production rate estimates.

## 3. Calibration Sites

Calibration sites were selected primarily based on the documentation of a well-constrained exposure history. Another consideration in their selection was whether the rock types present at a given site contained appropriate target elements to allow analysis of all commonly measured TCNs. The sites were also chosen to minimize potential factors that could affect the production rate calibrations, such as erosion, burial by snow or regolith, or prior exposure. Sample selection at each site also focused on mitigating the potential effects of outcrop/boulder geometry (Gosse and Phillips, 2001; Masarik and Weiler, 2003).

### *3.1. Lake Bonneville Shorelines*

Well-dated bedrock surfaces in northwestern Utah and southern Idaho associated with Pleistocene Lake Bonneville provide a unique opportunity for TCN production rate calibration (Oviatt et al., 1992). In the past, these surfaces have been used to estimate late Quaternary production rates for several nuclides, including  $^3\text{He}$  (Cerling, 1990; Cerling and Craig, 1994),  $^{10}\text{Be}$  (Poreda and Cerling, 1992),  $^{36}\text{Cl}$  (Phillips et al., 1996; Stone et al., 1996; Zreda et al., 1991), and  $^{14}\text{C}$  (Handwerger et al., 1999; Lifton et al., 2001; Miller et al., 2006). To provide a basis for intercomparison between the production rates for commonly measured TCNs, and to ensure that the most current techniques are employed in both sampling and laboratory procedures, key locations within the Lake Bonneville basin were re-sampled by CRONUS-Earth during the summer of 2005 (Figure 1).

The Lake Bonneville basin is characterized by a series of wave-cut bedrock benches and depositional shoreline features which formed during stillstands of the lake. The chronology of Lake Bonneville has been studied in depth and is extremely well constrained by numerous radiocarbon ages (Benson et al., 1990; Oviatt et al., 1992; Godsey et al., 2005). The Lake Bonneville highstand (known as the Bonneville level) is well preserved as the Bonneville

shoreline. This highstand is constrained in age by several radiocarbon dates ranging between 18.9 and 17.2 cal ka (Oviatt et al., 1992). The Bonneville shoreline is unique in that it was abandoned essentially instantaneously due to a catastrophic failure of the lake threshold at Red Rock Pass in southern Idaho, resulting in the Bonneville Flood (O'Connor, 1993). The resulting ~100 m drop in lake level led to the formation of the Provo shoreline (Oviatt et al., 1992; Godsey et al., 2005). The Bonneville Flood (and resulting abandonment of the Bonneville shoreline) has been precisely radiocarbon dated to  $17.4 \pm 0.2$  cal ka (Oviatt et al., 1992, calibrated using CALIB 5.01 (Reimer et al. 2004)), which we take as the exposure age of our samples.

The cut bedrock benches at Promontory Point are among the largest in the Bonneville basin, measuring hundreds of meters in width, with between 50-100 m (based on topographic map estimates) of overburden removed (Figure 3). These large-scale erosional features limit the possibility of significant TCN inheritance. The surfaces are well preserved and exhibit primary wave-rounding/polishing. Quartzites and quartzite conglomerates crop out at the site, allowing measurement of several common TCNs, including  $^{10}\text{Be}$ ,  $^{26}\text{Al}$ ,  $^{14}\text{C}$ ,  $^{21}\text{Ne}$ , and  $^{36}\text{Cl}$ . We analyzed six samples from the Bonneville shoreline benches at Promontory Point (Figures 1 and 2, Table 1) for in situ  $^{14}\text{C}$ . The samples were collected along a transect approximately perpendicular to the cut bedrock cliff face to test for any effects of differential shielding by overburden (Figure 2). Samples were taken from bedrock outcrops and large boulders exhibiting primary wave-polish (Figure 4).

### *3.2. Northwestern Scottish Highlands*

To date, TCN production rates in northwestern Scotland have been estimated for only  $^{10}\text{Be}$  (Stone et al., 1998) and  $^{36}\text{Cl}$  (Ballantyne et al., 1998), based on glacial moraine deposits. Late-Glacial-age (~11.6 cal ka) landslide deposits in northwestern Scotland provide a second,

unique opportunity for TCN production rate calibration. The deposits consist of large, angular boulders, deposited directly onto the surfaces of glaciers, and then left as lags when the glaciers retreated. Although there are no independent dates on these deposits, the timing of the landslide events can be constrained by the chronologies of the transporting glaciers. Under CRONUS-Earth, two landslide sites were sampled in the northwestern Highlands (Figure 5): Corrie nan Arr (Figure 6) and Maol Chean-dearg (Figure 7). The sites were sampled in the summer of 2006 (Table 1).

Northwestern Scotland is marked by glacial landforms and deposits that formed during the last global ice age. At its maximum extent (~17-18 cal ka), the last British ice sheet covered approximately two-thirds of the British Isles, including a majority of the Scottish Highlands (Stone *et al.*, 1998). After the final glacial retreat at the close of the last ice age (around 15.5 cal ka), a short-lived glacial readvance occurred between ~12.9-11.6 cal ka, known as the Loch Lomond Readvance (LLR) (Younger Dryas equivalent). The LLR was the last known period during which the Scottish Highlands were occupied by glaciers. Many studies have been devoted to determining the extent, thickness, and timing of ice coverage in northwestern Scotland (Ballantyne, 1997; 2007; Boulton *et al.*, 1977; Boulton *et al.*, 1991; Golledge, 2007; Golledge and Hubbard, 2005; Golledge *et al.*, 2008; Hubbard, 1997; 1999; Lukas and Benn, 2006; McCarroll *et al.*, 1995; Phillips *et al.*, 2006; Stone *et al.*, 1998), and various proxies have been used to constrain the timing of the final retreat of the glaciers to ~11.6 cal ka (e.g., GRIP ice core (Johnsen *et al.*, 1992), GISP2 ice core (Alley *et al.*, 1993), lake chronologies and pollen reconstructions (Charman, 1994; Walker and Lowe, 1987), chironomid reconstructions (Brooks and Birks, 2000; 2001), and the presence of the Vedde Ash layer (dated at  $11.98 \pm 0.08$  GRIP ice-core kyr BP) in peat bog cores on the Isle of Skye (Davies *et al.*, 2001)).

Due to its proximity to the North Atlantic, northwestern Scotland is very sensitive to climate changes in that region. As a result, small alpine glaciers in Scotland have responded rapidly to regional climatic variations (e.g. Dyurgerov and Meier, 2000; Lowell, 2000). The Greenland ice-cores (GRIP and GISP) provide a valuable record of climate change in the North Atlantic region, and can be correlated to climate changes in northwestern Scotland. Distinct  $\delta^{18}\text{O}$  excursions in the Greenland ice cores can therefore be correlated to specific glacial moraines in northwestern Scotland formed during the LLR. As a result, the ~1300 year LLR event can be subdivided into smaller periods of time, during which individual moraines formed. The innermost moraines of LLR glaciated valleys should thus date to the timing of final deglaciation at ~11.6 cal ka.

Corrie nan Arr and Maol Chean-dearg are previously glaciated valleys in the Scottish Highlands. Detailed geomorphologic mapping of glacial limits and landforms has been done at Corrie nan Arr (Jones, 1998), and both sites fall within the maximum extent of LLR glaciers (e.g., Golledge *et al.*, 2008; Hubbard, 1998; Jones, 1998; Hubbard, 1997). Thus, we believe moraine sequences at these sites correspond to events of the LLR. The landslide deposits sampled in this study lay within the limits of the innermost LLR glacier terminus deposits. If the landslide events had occurred during the initial stages of the LLR or earlier, the deposits would have been overridden by LLR or earlier glaciers and reworked to form standard glacial deposits. However, the preservation of the angular landslide blocks, and their location relative to LLR glacial deposits, lead us to conclude that they are associated with the final glacial retreat of the LLR. Therefore, we adopt the currently accepted age for the end of the LLR ( $11.6 \pm 0.2$  cal ka) as the age of our samples.

We analyzed three arkosic sandstone samples from Corrie nan Arr (Figure 6, Table 1) and seven quartzite samples from Maol Chean-dearg (Figure 7, Table 1) for in situ  $^{14}\text{C}$ . Samples were generally collected from angular boulders (a characteristic used to distinguish landslide boulders from glacially rounded boulders present at the same sites), although one sample was collected at Corrie nan Arr from a polished, somewhat rounded boulder as well. We only collected samples from large boulders (Table 1), minimizing the potential for significant inheritance in the samples while increasing the likelihood of boulder stability since the glacial ice disappeared.

## 4. Methods

### 4.1. Physical and Chemical Pretreatment

Each rock sample was crushed and homogenized at the Purdue Rare Isotope Measurement Laboratory (PRIMELab), and then divided into smaller aliquots for distribution to multiple investigators for analysis. The samples for in situ  $^{14}\text{C}$  extraction were sieved to separate the 0.25-0.50 mm size fraction to minimize  $^{14}\text{CO}_2$  adsorption from the atmosphere (Barker and Torkelson, 1975; Graham et al., 1979; Lifton et al., 2001; Roman, 1989) and yet allow complete extraction of in situ  $^{14}\text{C}$ . Pure quartz was isolated from each sample following the procedures established by Kohl and Nishiizumi (1992) and Lifton et al. (2001). Samples were sonicated for nine hours/day in a 1% HF/1%  $\text{HNO}_3$  solution at 95°C for four days (with fresh solution each day), instead of one day as described in Lifton et al. (2001).

The remaining high-purity quartz samples were then dried in a vacuum oven at 75°C, cooled to room temperature, and stored in clean glass jars. To eliminate any atmospheric  $\text{CO}_2$  contamination potentially acquired during storage, the day before  $^{14}\text{C}$  extraction, each sample was sonicated for 30 minutes at room temperature in a 1:1 mixture of concentrated  $\text{HNO}_3$  and 18

MΩ water, followed by an additional 90-minute leach without sonication. Each sample was then rinsed thoroughly and dried overnight in a vacuum oven at 75°C (Lifton et al., 2001).

#### 4.2. Isotopic Extraction

In situ  $^{14}\text{C}$  was extracted from each sample using techniques described by Lifton et al. (2001), Pigati (2004), and Miller et al. (2006). Two separate systems were used for extraction in this study: the recirculating system described by Lifton et al. (2001) and the flow-through system described by Pigati (2004). The general extraction procedures outlined below were used for both systems. The flow-through extraction system was used on all but two samples in this study; the remaining two samples were extracted using the recirculating system.

Briefly, a degassed lithium metaborate flux ( $\text{LiBO}_2$ ) was used to dissolve each quartz sample in an atmosphere of ~50 torr of Research Grade (RG)  $\text{O}_2$ , in a two-day process. Day one of the extraction procedure focused on removing contaminant gases from approximately 20 g of  $\text{LiBO}_2$  by combustion in RG  $\text{O}_2$  for one hour at 1200°C. All evolved gases were collected with liquid nitrogen (LN) and subsequently discarded. The  $\text{LiBO}_2$  was then allowed to cool overnight. The following day, ~5.0 g of quartz was added to the  $\text{LiBO}_2$  and was subjected to a two-step combustion in RG  $\text{O}_2$ . First, the sample was combusted for one hour at 500°C, to remove any remaining atmospheric or organic C. The sample was then combusted for three hours at 1100°C, dissolving the quartz in the  $\text{LiBO}_2$ , releasing the in situ  $^{14}\text{C}$ . All evolved C species were oxidized to  $\text{CO}_2$  and trapped with LN. The evolved gases were then subjected to a rigorous gas cleanup procedure (to remove gases other than  $\text{CO}_2$ ) and diluted with  $^{14}\text{C}$ -free  $\text{CO}_2$  (Tables 2 and 3). The diluted gas was converted to graphite using graphitization systems dedicated solely to in situ  $^{14}\text{C}$  samples to avoid potential higher-level  $^{14}\text{C}$  sample memory effects

(Lifton et al., 2001). Finally, the  $^{14}\text{C}$  content of the samples was analyzed at the Arizona Accelerator Mass Spectrometry (AMS) Laboratory.

#### 4.3. *In situ* $^{14}\text{C}$ Concentrations

The concentration of  $^{14}\text{C}$  atoms per gram of sample collected in a given combustion step ( $C_{14}$ ) is given by

$$C_{14} = \frac{\left( \frac{F_m A_{14} N_A V_S}{V_A} - B \right)}{M} \quad (4)$$

where  $F_m$  is the fraction modern (the  $^{14}\text{C}/^{13}\text{C}$  ratio of the sample vs. that of a standard, both corrected to  $\delta^{13}\text{C} = -25\text{‰}$  VPDB and to A.D. 1950),  $A_{14}$  is the fractional abundance of  $^{14}\text{C}$  in “modern” carbon ( $1.177 \times 10^{-12} \text{ }^{14}\text{C}/^{12}\text{C}$ ),  $V_S$  is the volume of  $\text{CO}_2$  in cc STP collected from the sample in a given combustion step,  $V_A$  is the volume of one mol of  $\text{CO}_2$  in cc STP,  $N_A$  is Avogadro’s number,  $M$  is the sample mass in g (set to one for blanks) (Jull et al., 1989; Lifton et al., 2001), and  $B$  is the number of  $^{14}\text{C}$  atoms associated with the corresponding extraction blank.  $B$  is determined by following the same extraction techniques used to analyze a sample, however no quartz sample is added on day two of the procedure. Extraction blanks thus represent the number of  $^{14}\text{C}$  atoms introduced into the system from sources other than the sample. The  $F_m$  value used is corrected for the mass-dependent graphitization blank following Lifton et al. (2001).

All measurement uncertainties from all aspects of our extraction and analytical procedures have been fully propagated through each calculation using the law of combination of errors, neglecting covariance terms (Bevington and Robinson, 1992). When averaging measured values, we use weighted means unless otherwise noted (Bevington and Robinson, 1992, Eqn. 4.17). We then calculate the uncertainty in the weighted mean (Bevington and Robinson, 1992,

Eqn. 4.19) and the weighted average variance of the data (Bevington and Robinson, 1992, Eqn. 4.22). We accept the larger of these uncertainties as the uncertainty in the weighted mean. All mean values are weighted using relative uncertainties instead of absolute uncertainties to minimize biases arising from correlated measurements and uncertainties. All uncertainties are presented as  $1\sigma$  unless otherwise noted.

## 5. Results

### 5.1. Measured Concentrations

Sample results are presented in Tables 2 and 3. Blank data used in our calculations are given in Appendix A. All measured sample concentrations have been normalized to the ground surface and no topographic shielding (Tables 1, 2, and 3) to allow inter-sample comparisons at each site.

#### 5.1.1. Bonneville Shoreline Site

Samples 05PPT-02, 05PPT-04, and 05PPT-05 were each analyzed twice. The measured concentrations from sample 05PPT-02 are indistinguishable at  $1\sigma$ . Replicate measured concentrations for sample 05PPT-04 overlap with the weighted mean for that sample at the  $2\sigma$  level, while replicate measured concentrations for 05PPT-05 overlap with its weighted mean at the  $1\sigma$  level. The weighted means for these samples were combined with the remaining samples (analyzed only once), to calculate overall site weighted mean concentrations.

The weighted mean concentration for the Lake Bonneville site, using all six samples, is  $(3.6100 \pm 0.0972) \times 10^5$   $^{14}\text{C}$  atoms  $(\text{g SiO}_2)^{-1}$  (Table 2). However, the concentration of sample 05PPT-02 does not agree with this value at the  $2\sigma$  level. A logical explanation for the low concentration would be that the sample was shielded in some manner (possibly by snow or regolith) for a significant amount of time, while the other samples were not. However, this is

unlikely because 05PPT-02 was collected approximately two meters from 05PPT-01, from a higher position on the same outcrop. Although the specific cause of the lower concentration of 05PPT-02 is unclear, the value is reproducible. Therefore, we consider 05PPT-02 a statistical outlier, and exclude it from subsequent analyses. The resulting weighted mean concentration for this site, excluding 05PPT-02, is  $(3.7339 \pm 0.0539) \times 10^5 \text{ }^{14}\text{C atoms (g SiO}_2\text{)}^{-1}$  (n=5).

### 5.1.2. Northwestern Scotland Sites

The three samples collected from Corrie nan Arr have in situ  $^{14}\text{C}$  concentrations that are indistinguishable from the site weighted mean at the  $1\sigma$  level. Sample 06HKY-04 was collected from a subglacial boulder, upvalley from the other samples, yet its concentration of in situ  $^{14}\text{C}$  agrees well with the others. This supports the validity of our assumption that the landslide blocks were approximately coeval with the glacial retreat. The weighted mean concentration for the site is  $(1.1874 \pm 0.0350) \times 10^5 \text{ }^{14}\text{C atoms (g SiO}_2\text{)}^{-1}$  (n=3).

Of the seven samples collected from Maol Chean-dearg, sample 06HKY-05 was analyzed three times for in situ  $^{14}\text{C}$  and sample 06HKY-06 was analyzed twice. The replicate measured concentrations for samples 06HKY-05 and 06HKY-06 overlap with their respective weighted means at the  $2\sigma$  level. The weighted means for these samples were combined with the remaining samples (analyzed only once), to calculate an overall site weighted mean concentration of  $(1.5280 \pm 0.0280) \times 10^5 \text{ }^{14}\text{C atoms (g SiO}_2\text{)}^{-1}$  (n=7).

## *5.2. Sampling Site Production Rate Estimates*

### 5.2.1. Bonneville Shoreline Site

Samples from Promontory Point were collected from surfaces with evidence of no erosion (i.e., wave polishing (Figure 4)), thus we did not correct for the effects of erosion in our

production rate calculations. Furthermore, no corrections were made for inheritance or snow cover, following the arguments of Lifton et al. (2001).

Site production rates calculated for the Promontory Point samples in this study (excluding 05PPT-02), all overlap with the weighted mean for this site at  $1\sigma$ , with the exception of 05PPT-04 (Table 2). We take the weighted mean in situ  $^{14}\text{C}$  production rate of  $51.4 \pm 0.8$   $^{14}\text{C}$  atoms ( $\text{g SiO}_2$ ) $^{-1}$   $\text{y}^{-1}$  ( $n=5$ ) as our best estimate for this site. This estimate falls between the earlier weighted mean production rate estimates of Lifton et al. (2001) and Miller et al. (2006) for a sample from the same site. We argue that our new value is a more representative estimate for this site, as it incorporates natural sample-to-sample variability in addition to analytical uncertainties.

Handwerger et al. (1999) also estimated in situ  $^{14}\text{C}$  production rates for Lake Bonneville, based on measurements made on calcite collected from the Provo level shoreline, which resulted from a period of stability immediately after the Bonneville flood (Oviatt et al., 1992). Handwerger et al. (1999) assumed a calibrated  $^{14}\text{C}$  age of 17.5 cal ka for their sites at  $40^\circ\text{N}$  latitude on the Provo shoreline. Based on this, they estimated an in situ  $^{14}\text{C}$  production rate at their calibration site of  $56 \pm 10$  atoms ( $\text{g CaCO}_3$ ) $^{-1}$   $\text{y}^{-1}$ . Godsey et al. (2005), however, recently published a revised estimate of the age of abandonment of the Provo shoreline of approximately 12  $^{14}\text{C}$  ka ( $14.4 \pm 0.4$  cal ka). Using this revised age for the exposure duration yields a mean site production rate (unweighted average  $\pm 1\sigma$  standard deviation) of  $59.4 \pm 10.4$  atoms ( $\text{g CaCO}_3$ ) $^{-1}$   $\text{y}^{-1}$ . The weighted average is  $57.7 \pm 4.0$  atoms ( $\text{g CaCO}_3$ ) $^{-1}$   $\text{y}^{-1}$ , which agrees at the  $2\sigma$  level with our weighted mean production rate for Promontory Point. However, the history of the Provo shoreline is apparently more complex than that of the Bonneville shoreline. Therefore, we argue that our Bonneville shoreline production rate estimates are likely more robust.

As mentioned in Section 3.1, the samples at Promontory Point were collected along a transect approximately perpendicular to the wave-cut cliff face to test for any effects of differential shielding by overburden (Figure 2). Our results do not indicate any significant differential shielding effect on in situ  $^{14}\text{C}$  production at this site.

### 5.2.2. Northwestern Scotland Sites

Samples from northwestern Scotland were collected from boulder surfaces exhibiting evidence of minimal erosion (e.g., resistant mineral veins, lack of weathered pits). Therefore, we did not correct for the effects of erosion in our production rate calculations. Samples are unlikely to contain an inherited signal, as only one surface on each boulder may possibly have been exposed on a pre-existing cliff face prior to the landslide. If such a surface was sampled, TCN concentrations should clearly present the sample as an outlier. As such, we did not correct for inheritance in our samples.

We also investigated whether snow cover corrections were needed for the two Scottish sites. Corrie nan Arr and Maol Chean-dearg currently experience relatively mild climates year-round due to their low altitudes and proximity to the western coast of Scotland. We also investigated snow cover records from the Scottish Executive Central Research Unit (2000). We examined data available from 1961-1990 for several stations geographically similar to Corrie nan Arr (near the west coast at low altitude). Mean snow cover duration for the period of record ranged from 11-20 days. No stations were present in western Scotland at altitudes representative of Maol Chean-dearg (~500 m). Given its proximity to Corrie nan Arr, however, we assume snow cover at the two sites should be similar. Therefore, we consider the likelihood of extended snow cover in the past as limited. We were unable to obtain data on the mean snow depth in the vicinity of our sites. However, as a precaution, we took care to sample the largest and tallest

boulders available at each site (Figures 6B and 7B), assuming that this would limit the possibility of extended deep snow cover. We thus did not correct for potential snow cover effects in these samples.

Production rate estimates are presented in Table 3. Individual sample estimates for Corrie nan Arr and Maol Chean-dearg overlap their respective weighted means of  $19.0 \pm 0.6$   $^{14}\text{C}$  atoms  $(\text{g SiO}_2)^{-1} \text{y}^{-1}$  (Corrie nan Arr (n=3)), and  $24.5 \pm 0.5$   $^{14}\text{C}$  atoms  $(\text{g SiO}_2)^{-1} \text{y}^{-1}$  (Maol Chean-dearg (n=7)) at the  $2\sigma$  level.

Of our three sites, sample production rates determined for Corrie nan Arr show the least scatter, while those for Promontory Point show the most. Our results for Corrie nan Arr, however, consist of only three analyses. As a result, the production rate uncertainty at that site may not be as representative of the potential sample-to-sample variability as the uncertainties at the other sites with more analyses. For example, fewer samples allow for less laboratory handling and decrease possibilities for sample-to-sample variability. Overall, the scatter at each site is comparable with that of earlier measurements (e.g., Lifton et al., 2001; Miller et al., 2006). We therefore consider our weighted mean site production rate estimates to be representative for each site.

### *5.3. Sea Level, High Latitude Production Rate Estimates*

An essential tool in TCN applications is the ability to scale TCN production rates from well-constrained calibration sites to sites under study. The intensity of the cosmic-ray flux responsible for TCN production varies with both altitude and position within the geomagnetic field. As such, scaling models accounting for such variations are necessary to estimate production rates accurately where calibrated estimates are not available.

Site specific production rate estimates are typically scaled to values at sea level and high (>60°) geomagnetic latitudes (SLHL) for comparison to production rates of other TCNs. This is because at geomagnetic latitudes greater than approximately 60°, the cosmic-ray flux is unaffected by changes in geomagnetic field strength, and therefore depends solely on altitude (Lal, 1991). TCNs may have multiple significant production mechanisms (e.g., spallogenic production, muogenic production) with different scaling characteristics. In this case, each mechanism should be scaled separately. In situ  $^{14}\text{C}$  is produced dominantly by spallation, with lesser production by fast muon interactions and slow muon capture. The proportions of these mechanisms for in situ  $^{14}\text{C}$  have not been directly measured in natural samples, thus we assume the SLHL production proportions of Heisinger *et al.* (2002): 83% spallation, 2% fast muon interactions, and 15% slow muon capture.

Four TCN scaling models describing atmospheric cosmic-ray variations have been published to date. Since each is based on different assumptions and parameterizations, they typically yield different values to SLHL production rates. It is critical to note that these values are not interchangeable. That is, if one uses a given scaling model with a given set of assumptions (e.g., atmospheric structure, geomagnetic model), then one must only use the SLHL production rate values that have been derived using the same scaling model and assumptions. Hence, we calculate SLHL values for in situ  $^{14}\text{C}$  production for each of the four scaling models, using a consistent set of assumptions.

Lal (1991) developed the first TCN scaling model, based on the variation in atmospheric nuclear disintegration rates with geomagnetic latitude and altitude. This model is typically applied with the assumption that for time periods exceeding several thousand years, the geomagnetic field averages to a geocentric axial dipole, or GAD. In this case, geomagnetic and

geographic latitudes are equivalent. Stone (2000) reparameterized this model as a function of atmospheric pressure (instead of altitude), to account for regional differences in mean annual atmospheric pressures. This is the simplest of the four scaling models, as it does not consider effects of temporal variation of the Earth's geomagnetic field. The model is typically applied with the assumption that nuclide production rates have been constant. However, since the geomagnetic field has indeed, varied through time, this assumption is invalid. Subsequent scaling models, thus, were developed in an attempt to incorporate geomagnetic effects and other temporal variability.

Scaling models by Dunai (2001), Desilets and Zreda (2003) (extended by Desilets et al. (2006) based on new, low latitude measurements), and Lifton et al. (2005) have been developed since that of Lal (1991). Each of these models is based on neutron monitor data, while Dunai (2001) also incorporates cloud chamber data. Each model is parameterized in terms of atmospheric depth and some form of effective vertical cutoff rigidity,  $R_C$ . Cutoff rigidity ( $R$ ) is defined as the minimum rigidity (momentum-to-charge ratio) that primary cosmic rays must have to penetrate the Earth's magnetic field at a given location.  $R_C$  expands on this definition by accounting for the effects of the zone of alternating allowed and forbidden cosmic-ray trajectories near the Earth known as the penumbral region. This region results from the interaction of complex, looping cosmic-ray trajectories with the solid Earth (Cooke et al., 1991; Shea et al., 1965). The most accurate way to estimate  $R_C$  is with the method known as trajectory tracing, in which an anti-proton is numerically traced from the top of the Earth's atmosphere outward through a high-order spherical harmonic representation of the geomagnetic field (e.g., Shea et al., 1965).  $R_C$  is influenced by both dipole and non-dipole components of the geomagnetic field, and as a result, varies both spatially and temporally.

Each of these more recent scaling models features a means of estimating the effects of temporal and spatial geomagnetic variation on  $R_C$ . Dunai (2001) incorporates a dipolar approximation of  $R_C$ , using geomagnetic inclination and horizontal field intensity to address local non-dipole field variations. Desilets and Zreda (2003) and Lifton et al. (2005) are both based on trajectory-derived  $R_C$  values. Desilets and Zreda (2003) utilize trajectory-traced  $R_C$  values derived for a GAD field of varying intensity, as a function of geomagnetic latitude. This approach attempts to tie together modern trajectory-derived values used for ordering the neutron monitor data and trajectory-derived values appropriate for long-term mean geomagnetic conditions. Lifton et al. (2005) attempted to account for potentially persistent non-dipole field effects on  $R_C$  by fitting a quasi-dipolar model to a global grid of trajectory-traced  $R_C$  values derived for the 1955.0 geomagnetic epoch (Shea et al., 1968). Lifton et al. (2005) also utilized a much larger neutron monitor dataset than the other two models, explicitly accounting for the effects of solar modulation on the cosmic-ray flux.

However, these models of  $R_C$  variation risk systematic errors by using simplified (generally dipolar) paleomagnetic models to drive scaling models parameterized with  $R_C$  values derived from detailed modern geomagnetic field representations. Lifton et al. (2008) used a continuous geomagnetic model covering the last 7 ka as a basis for a new geomagnetic framework to quantify temporal and spatial  $R_C$  variations, in an attempt to minimize such systematic errors. The framework incorporates globally gridded trajectory-traced  $R_C$  values spaced over the last 7 ka, and a model of trajectory-traced  $R_C$  variation with paleointensity for periods beyond 7 ka.

We use this geomagnetic framework in each of the latter three scaling models to calculate our SLHL production rates, while we assume a GAD for the Lal (1991)/Stone (2000) model.

Following Balco et al. (2008), we also consider an additional geomagnetic input for the Lal (1991)/Stone (2000) scaling model, in an effort to separate differences in altitude scaling from differences between time-dependent and non-time-dependent geomagnetic models. This input varies the geomagnetic field assuming the geocentric dipole (GD – i.e., variation in pole position and dipolar intensity only), using values derived from the Lifton et al. (2008) framework per Balco et al. (2008).

### 5.3.1. In situ $^{14}\text{C}$ Production Rate Estimates at SLHL

SLHL-scaled production rate results are shown in Table 4. For comparison, we scaled weighted mean production rate estimates for Lake Bonneville from Lifton et al. (2001) and Miller et al. (2006) to SLHL as well. We then calculated an overall, unweighted mean for each scaling model from the scaled, weighted mean production rate estimates from each of the three sites in this study, following the approach of Balco et al. (2008). At present, these values represent our best estimates of reference in situ  $^{14}\text{C}$  production rates based on the calibration sites in this study.

Promontory Point SLHL-scaled weighted mean estimates for all five models fall between the previous estimates of Lifton et al. (2001) and Miller et al. (2006). All of the models predict weighted mean estimates for Promontory Point (this study) that agree with the Lifton et al. (2001) estimates at the  $1\sigma$  level, while only the Dunai (2001) estimate agrees with the Miller et al. (2006) estimate at the  $2\sigma$  level.

For all models, the Corrie nan Arr SLHL-scaled weighted mean estimates do not differ significantly at the  $2\sigma$  level from the Lifton et al. (2001) weighted mean estimates. With the exception of the Lal (1991)/Stone (2000) geomagnetic model, the remaining model estimates also agree with the Miller et al. (2006) estimates at the  $2\sigma$  level. The SLHL-scaled weighted

mean estimates for Corrie nan Arr and Promontory Point (this study) for all models agree at the  $2\sigma$  level.

Maol Chean-dearg SLHL-scaled weighted mean estimates all fall below the previous estimates of Lifton et al. (2001) and Miller et al. (2006). Only the Lal (1991)/Stone (2000) geomagnetic model and Dunai (2001) model estimates agrees at  $2\sigma$  with the previous estimates of Miller et al. (2006). The weighted mean results for Maol Chean-dearg and Corrie nan Arr do not differ significantly at the  $2\sigma$  level using only the Lifton et al. (2005) model. None of the model estimates for Maol Chean-dearg agrees at  $2\sigma$  with the corresponding estimates for Promontory Point (this study).

Unweighted mean ( $\pm 1\sigma$  standard error) estimates for our three sites range from  $15.63 \pm 0.41$   $^{14}\text{C}$  atoms  $(\text{g SiO}_2)^{-1} \text{y}^{-1}$  (Lal (1991)/Stone (2000) with geomagnetic variation) to  $17.77 \pm 0.57$   $^{14}\text{C}$  atoms  $(\text{g SiO}_2)^{-1} \text{y}^{-1}$  (Lifton et al. (2005)). Lifton et al. (2005) model estimates are higher than the other model estimates for each individual site as well. This is because that model accounts for the effects of solar modulation, which in contrast to geomagnetic effects, affect the cosmic-ray flux mostly at the high latitudes to which we are scaling. All scaling models yield 2-4% standard errors on the unweighted means – well within the stated 5% ( $1\sigma$ ) uncertainty goal of CRONUS-Earth. Furthermore, our three site weighted means overlap at  $2\sigma$  with the unweighted mean for all five models.

The unweighted mean production rate estimates using each model generally fall between the corresponding previous estimates of Lifton et al. (2001) and Miller et al. (2006), except for that of Lifton et al. (2005), which is below both. Unweighted mean estimates for all five models overlap their respective Lifton et al. (2001) and Miller et al. (2006) weighted mean estimates at the  $2\sigma$  level. As suggested by Miller et al. (2006), the more complicated extraction procedures of

Lifton *et al.* (2001) might have allowed more opportunities to inadvertently introduce small amounts of contaminant  $^{14}\text{C}$ , potentially leading to production rate overestimates. Miller *et al.* (2006) estimates are based on multiple analyses of a single sample; therefore, their estimates may be biased by characteristics specific to the sample. Therefore, we favor our estimates because they are based on a number of samples from multiple sites, and thus mitigate such potential biases. Furthermore, our results demonstrate the importance of using multiple calibration sites for SLHL scaling, as individual sites may yield SLHL-scaled production rates which are distinguishable from one another at varying levels.

## 6. Conclusions

We have estimated *in situ*  $^{14}\text{C}$  production rates for two calibration sites: Lake Bonneville, Utah and northwestern Scotland. We analyzed several samples from each site (six from Lake Bonneville, three from Corrie nan Arr, and seven from Maol Chean-dearg) using the extraction techniques recently developed by Lifton *et al.* (2001) and Pigati (2004), as well as a more robust pretreatment. We argue that the consistency with which we selected, processed, and analyzed each sample, combined with our use of multiple samples from multiple sites, helps to minimize uncertainties and sample- and site-specific biases. Our new results, therefore, should improve on existing *in situ*  $^{14}\text{C}$  production rate estimates.

We found *in situ*  $^{14}\text{C}$  concentration results between replicate analyses of single samples to be distinguishable from one another at the  $2\sigma$  level for all but one sample. We believe these inconsistencies may result from inhomogeneities remaining in pretreated samples and/or laboratory variability inherent to our procedures. Weighted means of our results, thus, incorporate these differences and yield production rate estimates that dampen natural and analytical variables. All of our sample production rate estimates from both Scottish sites fall

within  $2\sigma$  uncertainty of the weighted means for the respective sites, and all but one estimate from Promontory Point agree at the  $1\sigma$  level with the site weighted mean.

Our preferred site production rate estimate for the Bonneville shoreline at Promontory Point, Utah, falls between the previous estimates of Lifton *et al.* (2001) and Miller *et al.* (2006). As no previous estimates for in situ  $^{14}\text{C}$  production rates exist for northwestern Scotland, we rely on five different SLHL scaling models to compare our estimates from two sites in Scotland to one another and to our Lake Bonneville estimate. All models estimate that the unweighted mean for our three sites falls between the earlier estimates of Lifton *et al.* (2001) and Miller *et al.* (2006), except the Lifton *et al.* (2005) model estimate, which is lower than both. All scaling models yield 2-4% standard errors on the unweighted means, which is well within the stated 5% ( $1\sigma$ ) uncertainty goal of CRONUS-Earth. However, it is clear that production rate estimates and SLHL scaling models can only improve with more calibration data from additional sites. Analyses from additional CRONUS-Earth calibration sites are forthcoming, and when combined with the results of this study, should further improve in situ  $^{14}\text{C}$  production rate estimates. It is also important to note that as research continues on overall TCN systematics, potential improvements in scaling methods will require future revision of TCN SLHL production rates.

### **Acknowledgements**

This work was supported by NSF Grant EAR-0345150 (CRONUS-Earth Project), to Lifton and Jull, the University of Arizona's Accelerator Mass Spectrometry Laboratory, and the University of Arizona's Charles Evenson, Geosciences, and Wilson Thompson Scholarships to Dugan.

### **References**

- Alley, R.B., Meese, D.A., Shuman, C.A., Gow, A.J., Taylor, K.C., Grootes, P.M., White, J.W.C., Ram, M., Waddington, E.D., Mayewski, P.A., Zielinski, G.A., 1993. Abrupt increase in Greenland snow accumulation at the end of the Younger Dryas event. *Nature*. 362, 527-529.
- Balco, G., Stone, J.O., Lifton, N.A., Dunai, T.J., 2008. A complete and easily accessible means of calculating surface exposure ages or erosion rates from  $^{10}\text{Be}$  and  $^{26}\text{Al}$  measurements. *Quaternary Geochronology*. 3, 174-195.
- Ballantyne, C.K., 2007. Loch Lomond Stadial glaciers in North Harris, Outer Hebrides, North-West Scotland: glacier reconstruction and palaeoclimatic implications. *Quaternary Science Reviews*. 26, 3134-3149.
- Ballantyne, C.K., 1997. The periglacial geomorphology of Scotland, in: Gordon, J.E. (Ed.), *Reflections on the Ice Age in Scotland: an Update on Quaternary Studies*. Scottish Association of Geography Teachers and Scottish Natural Heritage, Glasgow, pp. 166-178.
- Ballantyne, C.K., Stone, J.O., Fifield, L.K., 1998. Cosmogenic  $\text{Cl-36}$  dating of postglacial landsliding at The Storr, Isle of Skye, Scotland. *The Holocene*. 8, 347-351.
- Barker, C. and Torkelson, B.E., 1975. Gas adsorption on crushed quartz and basalt. *Geochimica et Cosmochimica Acta*. 39, 212-218.
- Benson, L.V., Currey, D.R., Dorn, R.I., Lajoie, K.R., Oviatt, C.G., Robinson, S.W., Smith, G.I., Stine, S., 1990. Chronology of expansion and contraction of four great Basin lake systems during the past 35,000 years. *Palaeogeography, Palaeoclimatology, Palaeoecology*. 78, 241-286.

- Bevington, P.R. and Robinson, D.K., 1992. *Data Reduction and Error Analysis for the Physical Sciences*. McGraw-Hill, New York, N.Y.
- Boulton, G.S., Jones, A.S., Clayton, K.M., Kenning, M.J., 1977. A British ice-sheet model and patterns of glacial erosion and deposition in Britain, in: Shotton, F.W. (Ed.), *British Quaternary studies: Recent advances*. Clarendon Press, Oxford, pp. 231-246.
- Boulton, G.S., Peacock, J.D., Sutherland, D.G., 1991. Quaternary, in: Craig, G.Y. (Ed.), *Geology of Scotland*. The Geological Society, London, pp. 503-543.
- Brooks, S.J. and Birks, H.J.B., 2000. Chironomid-inferred late-glacial air temperatures at Whitrig Bog, southeast Scotland. *Journal of Quaternary Science*. 15, 759-764.
- Brooks, S.J. and Birks, H.J.B., 2001. Chironomid-inferred air temperatures from Lateglacial and Holocene sites in north-west Europe: progress and problems. *Quaternary Science Reviews*. 20, 1723-1741.
- Cerling, T.E., 1990. Dating geomorphologic surfaces using cosmogenic  $^3\text{He}$ . *Quaternary Research*. 33, 148-156.
- Cerling, T.E. and Craig, H., 1994. Cosmogenic  $^3\text{He}$  production rates from 39°N to 46°N latitude, western USA and France. *Geochimica et Cosmochimica Acta*. 58, 249-255.
- Charman, D.J., 1994. Late-glacial and holocene vegetation history of the flow country, northern Scotland. *New Phytologist*. 127, 155-168.
- Cooke, D.J., Humble, J.E., Shea, M.A., Smart, D.F., Lund, N., Rasmussen, I.L., Byrnek, B., Goret, P., Petrou, N., 1991. On cosmic-ray cut-off terminology. *Il Nuovo Cimento C*. 14(3), 213-234.

- Davies, S.M., Turney, Chris S.M., Lowe, J.J., 2001. Identification and significance of a visible, basalt-rich Vedde Ash layer in a Late-glacial sequence on the Isle of Skye, Inner Hebrides, Scotland. *Journal of Quaternary Science*. 16, 99-104.
- Desilets, D. and Zreda, M., 2003. Spatial and temporal distribution of secondary cosmic-ray nucleon intensities and applications to in situ cosmogenic dating. *Earth and Planetary Science Letters*. 206, 21-42.
- Desilets, D., Zreda, M., and Prabu, T., 2006. Extended scaling factors for in situ cosmogenic nuclides: New measurements at low latitude. *Earth and Planetary Science Letters*. 246, 265-276.
- Donahue, D.J., Linick, T.W., Jull, A.J.T., 1990. Isotope-ratio and background corrections for accelerator mass spectrometry radiocarbon measurements. *Radiocarbon*. 32, 135-142.
- Dunai, T.J., 2001. Influence of secular variation of the geomagnetic field on production rates of in situ produced cosmogenic nuclides. *Earth and Planetary Science Letters*. 193, 197-212.
- Dyurgerov, M.B. and Meier, M.F., 2000. Twentieth century climate change: Evidence from small glaciers. *Proceedings of the National Academy of Sciences of the United States of America*. 97, 1406-1411.
- Godsey, H.S., Currey, D.R., Chan, M.A., 2005. New evidence for an extended occupation of the Provo shoreline and implications for regional climate change, Pleistocene Lake Bonneville, Utah, USA. *Quaternary Research*. 63, 212-223.
- Golledge, N.R., 2007. Sedimentology, stratigraphy, and glacier dynamics, western Scottish Highlands. *Quaternary Research*. 68, 79-95.

- Golledge, N.R. and Hubbard, A., 2005. Evaluating Younger Dryas glacier reconstructions in part of the western Scottish Highlands: a combined empirical and theoretical approach. *Boreas*. 34, 274-286.
- Golledge, N.R., Hubbard, A., Sugden, D.E., 2008. High-resolution numerical simulation of Younger Dryas glaciation in Scotland. *Quaternary Science Reviews*. 27, 888-904.
- Gosse, J.C. and Phillips, F.M., 2001. Terrestrial in situ cosmogenic nuclides: theory and application. *Quaternary Science Reviews*. 20, 1475-1560.
- Graham, D.G., Muenow, D.W., Gibson, E.K., 1979. Some effects of gas adsorption on the high temperature volatile release behavior of a terrestrial basalt, tektite and lunar soil. *Lunar and Planetary Science Conference, 10th*. 2, 1617-1627.
- Handwerger, D.A., Cerling, T.E., and Bruhn, R.L., 1999. Cosmogenic <sup>14</sup>C in carbonate rocks. *Geomorphology*. 27, 13-24.
- Harrison, J., Winterbottom, S., Johnson, R., 2001. Climate change and changing patterns of snowfall in Scotland. A Research Publication of the Scottish Executive Central Research Unit, <http://www.scotland.gov.uk/Resource/Doc/156666/0042099.pdf>, 48 p.
- Heisinger, B., Lal, D., Jull, A.J.T., Kubik, P., Ivy-Ochs, S., Knie, K., Nolte, E., 2002. Production of selected cosmogenic radionuclides by muons: 2. Capture of negative muons. *Earth and Planetary Science Letters*. 200, 357-369.
- Hubbard, A., 1997. High resolution modelling of glacier flow. Ph.D. Dissertation, University of Edinburgh, Scotland.
- Hubbard, A., 1999. High-resolution modeling of the advance of the Younger Dryas ice sheet and its climate in Scotland. *Quaternary Research*. 52, 27-43.

- Johnsen, S.J., Clausen, H.B., Dansgaard, W., Fuhrer, K., Gunderstrup, N., Hammer, C.U., Iversen, P., Jouzel, J., Stauffer, B., Steffensen, J.P., 1992. Irregular glacial interstadials recorded in a new Greenland ice core. *Nature*. 359, 311-313.
- Jones, T., 1998. Empirical testing of Loch Lomond Stadial glacial limits derived from a glaciological model for the Applecross Peninsula, Wester Ross, Scotland. *Scottish Geographical Magazine*. 114, 164-171.
- Jull, A.J.T., Donahue, D.J., Linick, T.W., 1989. Carbon-14 activities in recently fallen meteorites and Antarctic meteorites. *Geochimica et Cosmochimica Acta*. 53, 2095-2100.
- Kohl, C.P. and Nishiizumi, K., 1992. Chemical isolation of quartz for measurement of in-situ - produced cosmogenic nuclides. *Geochimica et Cosmochimica Acta*. 56, 3583-3587.
- Lal, D., 1991. Cosmic ray labeling of erosion surfaces: in situ nuclide production rates and erosion models. *Earth and Planetary Science Letters*. 104, 424-439.
- Lifton, N.A., Bieber, J.W., Clem, J.M., Duldig, M.L., Evenson, P., Humble, J.E., Pyle, R., 2005. Addressing solar modulation and long-term uncertainties in scaling secondary cosmic rays for in situ cosmogenic nuclide applications. *Earth and Planetary Science Letters*. 239, 140-161.
- Lifton, N.A., Jull, A.J.T., Quade, J., 2001. A new extraction technique and production rate estimate for in situ cosmogenic  $^{14}\text{C}$  in quartz. *Geochimica et Cosmochimica Acta*. 65, 1953-1969.
- Lifton, N.A., Smart, D.F., Shea, M.A., 2008. Scaling time-integrated in situ cosmogenic nuclide production rates using a continuous geomagnetic model. *Earth and Planetary Science Letters*. 268, 190-201.

- Lowell, T.V., 2000. As climate changes, so do glaciers. *Proceedings of the National Academy of Sciences of the United States of America*. 97, 1351-1354.
- Lukas, S. and Benn, D.I., 2006. Retreat Dynamics of Younger Dryas Glaciers in the far NW Scottish Highlands Reconstructed from Moraine Sequences. *Scottish Geographical Journal*. 122, 308-325.
- Masarik, J. and Wieler, R., 2003. Production rates of cosmogenic nuclides in boulders. *Earth and Planetary Science Letters*. 216, 201-208.
- McCarroll, D., Ballantyne, C.K., Nesje, A., Dahl, S.O., 1995. Nunataks of the last ice sheet in northwestern Scotland. *Boreas*. 24, 305-323.
- Miller, G.H., Briner, J.P., Lifton, N.A., Finkel, R.C., 2006. Limited ice-sheet erosion and complex exposure histories derived from in situ cosmogenic  $^{10}\text{Be}$ ,  $^{26}\text{Al}$ , and  $^{14}\text{C}$  on Baffin Island, Arctic Canada. *Quaternary Geochronology*. 1, 74-85.
- Ordnance Survey, 2007a, Kyle of Lochalsh, Plockton, and Applecross. OS Explorer Map Sheet 428, 1:25,000.
- Ordnance Survey, 2007b, Glen Carron and West Monar. OS Explorer Map Sheet 429, 1:25,000.
- O'Connor, J.E., 1993. Hydrology, hydraulics, and geomorphology of the Bonneville flood. *Geological Society of America: Special Paper*. 274.
- Oviatt, C.G., 1997. Lake Bonneville fluctuations and global climate change. *Geology*. 25, 155-158.
- Oviatt, C.G., Currey, D.R., Sack, D., 1992. Radiocarbon chronology of Lake Bonneville, Eastern Great Basin, USA. *Palaeogeography, Palaeoclimatology, Palaeoecology*. 99, 225-241.

- Phillips, F.M., Zreda, M.G., Flinsch, M.R., Elmore, D., Sharma, P., 1996. A reevaluation of terrestrial rocks cosmogenic  $^{36}\text{Cl}$  production rates in terrestrial rocks. *Geophysical Research Letters*. 23, 949-952.
- Phillips, W.M., Hall, A.M., Mottram, R., Fifield, L.K., Sugden, D.E., 2006. Cosmogenic  $^{10}\text{Be}$  and  $^{26}\text{Al}$  exposure ages of tors and erratics, Cairngorm Mountains, Scotland: Timescales for the development of a classic landscape of selective linear glacial erosion. *Geomorphology*. 73, 222-245.
- Pigati, J.S., 2004. Experimental developments and application of carbon-14 and in situ cosmogenic nuclide dating techniques. Ph.D. Dissertation, University of Arizona, Tucson, 188 p.
- Poreda, R.J. and Cerling, T.E., 1992. Cosmogenic neon in recent lavas from the western United States. *Geophysical Research Letters*. 19, 1863-1866.
- Reimer, P.J., Baillie, M.G.L., Bard, E., Bayliss, A., Beck, J.W., Bertrand, C.J.H., Blackwell, P.G., Buck, C.E., Burr, G.S., Cutler, K.B., Damon, P.E., Edwards, R.L., Fairbanks, R.G., Friedrich, M., Guilderson, T.P., Hogg, A.G., Hughen, K.A., Kromer, B., McCormac, G., Manning, S., Ramsey, C.B., Reimer, R.W., Remmele, S., Southon, J.R., Suiver, M., Talamo, S., Taylor, F.W., van der Plicht, J., Weyhenmeyer, C.E., 2004. IntCal04 Terrestrial Radiocarbon Age Calibration, 0–26 cal ky BP. *Radiocarbon*. 46(3), 1029-1058.
- Roman, H., 1989. Measurements of in-situ production of  $^{14}\text{C}$  in  $\text{SiO}_2$ : Production rates and cross-sections.

- Shea, M.A., Smart, D.F., McCracken, K.G., 1965. A study of vertical cutoff rigidities using sixth degree simulations of the geomagnetic field. *Journal of Geophysical Research*. 70(17), 4117- 4130.
- Shea, M.A., Smart, D.F., McCall, J.R., 1968. A five degree by fifteen degree world grid of trajectory-determined vertical cutoff rigidities. *Canadian Journal of Physics*. 46, S1098-S1101.
- Stone, J.O., 2000. Air pressure and cosmogenic isotope production. *Journal of Geophysical Research*. 105, 23753-23759.
- Stone, J.O., Allan, G.L., Fifield, L.K., Cresswell, R.G., 1996. Cosmogenic chlorine-36 from calcium spallation. *Geochimica et Cosmochimica Acta*. 60, 679-692.
- Stone, J.O., Ballantyne, C.K., Keith Fifield, L., 1998. Exposure dating and validation of periglacial weathering limits, northwestern Scotland. *Geology*. 26, 587-590.
- U.S. Geological Survey, 2008. The National Map Seamless Server: DOQQ 1.0m B&W (West) UTM Zone 12 Orthoimagery. <http://seamless.usgs.gov/website/seamless/viewer/htm>.
- U.S. Geological Survey, 1991, Pokes Point, Utah, Quadrangle, 7.5 minute topographic series, 1:24,000.
- Walker, M.J.C. and Lowe, J.J., 1987. Flandrian environmental history of the Isle of Mull, Scotland. III. A high-resolution pollen profile from Gribun, western Mull. *New Phytologist*. 106, 333-347.
- Zreda, M.G., Phillips, F.M., Elmore, D., Kubik, P.W., Sharma, P., Dorn, R.I., 1991. Cosmogenic chlorine-36 production rates in terrestrial rocks. *Earth and Planetary Science Letters*. 105, 94-109.

**Figure Captions**

Figure 1. Vicinity map showing the maximum extent of Lake Bonneville relative to modern lakes and the Promontory Point sampling location.

Figure 2. Digital orthophoto of the Bonneville shoreline bench at Promontory Point, Utah, showing sample locations and geomorphic features. The black dotted line marks the major slope break delimiting the outer edge of the wave-cut bench. Geomorphic mapping by Fred Phillips. Base orthophoto from the US Geological Survey National Map Seamless Server (<http://seamless.usgs.gov/website/seamless/viewer/htm>).

Figure 3. Wave-cut bedrock bench at Bonneville shoreline, Promontory Point, Utah, looking north. The bench is approximately 300 m wide.

Figure 4. Example of characteristic wave polish on outcrops and boulders at Promontory Point.

Figure 5. Vicinity map showing northwestern Scotland sampling locations. Inset shows location within Great Britain.

Figure 6. (A) Map of the Corrie nan Arr sampling site, showing sample locations. Contour interval is 10 m. Source: Ordnance Survey, OS Explorer Map Sheet 428, 1:25,000.

(B) Sample 06HKY-04 was taken from the large boulder in the center of the photograph.

Figure 7. (A) Map of Maol Chean-dearg sampling site, showing sample locations. Contour interval is 10 m. Source: Ordnance Survey, OS Explorer Map Sheet 429, 1:25,000.

(B) Sample 06HKY-11 was taken from the flat top of the large boulder in the left-center of the picture.

## Tables

Table 1. Sample Data

	Sample ID	Latitude (°N)	Longitude (°E)	Altitude (m)	Rock Type and Boulder Dimensions (l, w, h) <sup>1</sup>	Sample Thickness $z$ (cm)	Thickness Correction Factor <sup>2</sup>	Shielding Correction Factor <sup>3</sup>
LAKE BONNEVILLE, UT								
Bonneville Shoreline at	05PPT-01	41.26367	-112.47527	1603 ± 5	Quartzite - Bedrock	3.0 ± 1.0	1.0255 ± 0.0050	1.0209 ± 0.0011
Promontory Point	05PPT-02	41.26367	-112.47527	1603 ± 5	Quartzite Conglomerate - Bedrock	3.0 ± 1.0	1.0255 ± 0.0050	1.0050 ± 0.0011
	05PPT-03	41.26356	-112.47580	1600 ± 5	Quartzite - Bedrock	3.0 ± 1.0	1.0255 ± 0.0050	1.0385 ± 0.0011
	05PPT-04	41.26362	-112.47693	1598 ± 5	Quartzite Conglomerate - Bedrock	2.5 ± 1.0	1.0171 ± 0.0050	1.0171 ± 0.0011
	05PPT-05	41.26390	-112.47498	1605 ± 5	Quartzite - Boulder (2.3, 2.0, 0.6)	4.0 ± 1.0	1.0341 ± 0.0050	1.0093 ± 0.0011
	05PPT-08	41.26379	-112.47476	1606 ± 5	Quartzite - Boulder (2.0, 1.8, 0.9)	2.5 ± 1.0	1.0212 ± 0.0050	1.0136 ± 0.0011
NW SCOTLAND								
Corrie nan Arr	06HKY-01	57.41523	-5.64637	134 ± 5	Arkosic Sandstone - Boulder (4.1, 4.0, 2.2)	2.0 ± 1.0	1.0163 ± 0.0050	1.0189 ± 0.0011
	06HKY-03	57.41550	-5.64662	131 ± 5	Arkosic Sandstone - Boulder (2.9, 2.4, 1.2)	6.7 ± 1.0	1.0554 ± 0.0050	1.0184 ± 0.0011
	06HKY-04	57.42302	-5.65808	137 ± 5	Arkosic Sandstone - Boulder (4.0, 3.8, 2.4)	4.0 ± 1.0	1.0329 ± 0.0050	1.0444 ± 0.0011
Maol-Chean-dearg	06HKY-05	57.48743	-5.44933	521 ± 5	Quartzite - Boulder (4.2, 1.6, 1.6)	3.5 ± 1.0	1.0298 ± 0.0050	1.0232 ± 0.0011
	06HKY-06	57.48755	-5.44978	527 ± 5	Quartzite - Boulder (3.4, 2.2, 0.9)	3.5 ± 1.0	1.0298 ± 0.0050	1.0341 ± 0.0011
	06HKY-07	57.48780	-5.44770	500 ± 5	Quartzite - Boulder (3.8, 1.8, 1.3)	6.5 ± 1.0	1.0558 ± 0.0050	1.0139 ± 0.0011
	06HKY-08	57.48863	-5.44705	502 ± 5	Quartzite - Boulder (NR)	3.0 ± 1.0	1.0255 ± 0.0050	1.0244 ± 0.0011
	06HKY-09	57.48863	-5.44705	502 ± 5	Quartzite - Boulder (NR)	5.0 ± 1.0	1.0428 ± 0.0050	1.0244 ± 0.0011
	06HKY-10	57.48732	-5.44863	510 ± 5	Quartzite - Boulder (2.3, 1.5, 1.3)	6.0 ± 1.0	1.0515 ± 0.0050	1.0187 ± 0.0011
	06HKY-11	57.48747	-5.44995	528 ± 5	Quartzite - Boulder (3.2, 1.3, 1.1)	4.5 ± 1.0	1.0384 ± 0.0050	1.0281 ± 0.0011

## Notes:

Latitude and longitude were recorded from a GPS receiver; altitudes were estimated from topographic maps (US Geological Survey, 1991; Ordnance Survey, 2007a and 2007b).

<sup>1</sup> Boulder dimensions given where applicable as (l, w, h), in m. NR = dimensions not recorded. Assumed densities: Quartzite and quartzite conglomerate –  $2.70 \pm 0.10 \text{ g cm}^{-3}$ ; Arkosic Sandstone –  $2.65 \pm 0.10 \text{ g cm}^{-3}$ .

<sup>2</sup> Thickness correction factor determined by  $(z\rho/\Lambda)/(1-e^{-z\rho/\Lambda})$ , where  $z$  is thickness in cm,  $\rho$  is density in  $\text{g cm}^{-3}$ , and  $\Lambda$  is taken to be  $160 \pm 10 \text{ g cm}^{-2}$ .

<sup>3</sup> Shielding correction factors determined using the CRONUS-Earth Online Geometric Shielding Calculator (Version 1.1. March, 2006. [http://hess.ess.washington.edu/math/general/skyline\\_input.php](http://hess.ess.washington.edu/math/general/skyline_input.php)).

Table 2. Sample Results and Production Rate Estimates for Lake Bonneville

Notes:

Sample Site	Sample	Lab number	AMS number	Mass of quartz analyzed (g) <sup>1</sup>	V <sub>CO2</sub> (ml)	Dilution Factor	F <sub>m</sub>	Normalized [ <sup>14</sup> C] (10 <sup>5</sup> <sup>14</sup> C atoms/g SiO <sub>2</sub> ) <sup>2</sup>	P <sub>0</sub> at Site ( <sup>14</sup> C atoms/g SiO <sub>2</sub> )/y
LAKE BONNEVILLE									
<i>Lifton et al. (2001)</i>	<b>Weighted Mean (n=6)<sup>3</sup></b>							<b>3.8306 ± 0.1344</b>	<b>52.9 ± 1.7</b>
<i>Miller et al. (2006)</i>	<b>Weighted Mean (n=10)</b>							<b>3.5687 ± 0.0510</b>	<b>49.2 ± 0.7</b>
<i>This Study</i>	05PPT-01	RN-883	AA-68804	4.99903	0.03836 ± 0.00052	38.53	0.0460 ± 0.0006	3.8234 ± 0.0848	52.7 ± 1.2
	05PPT-02a	RN-868	AA-68805	4.99912	0.03729 ± 0.00035	33.54	0.0487 ± 0.0011	3.3250 ± 0.1055	45.8 ± 1.5
	05PPT-02b	RN-911	AA-68805	5.00140	0.03502 ± 0.00025	46.19	0.0374 ± 0.0005	3.2797 ± 0.0786	45.2 ± 1.1
	05PPT-02								
	<i>Weighted Mean</i>							<i>3.2962 ± 0.0631</i>	<i>45.4 ± 0.9</i>
	05PPT-03	RN-866	AA-68806	4.99819	0.04955 ± 0.00045	27.90	0.0473 ± 0.0006	3.7245 ± 0.0829	51.3 ± 1.2
	05PPT-04a	RN-894	AA-68807	4.99735	0.04595 ± 0.00035	29.98	0.0465 ± 0.0005	3.5340 ± 0.0747	48.7 ± 1.1
	05PPT-04b	RN-912	AA-68807	4.99530	0.05020 ± 0.00034	32.24	0.0368 ± 0.0005	3.2355 ± 0.0789	44.6 ± 1.1
	05PPT-04								
	<i>Weighted Mean</i>							<i>3.4060 ± 0.1477</i>	<i>46.9 ± 2.0</i>
	05PPT-05a	RN-877	AA-68808	4.99497	0.04859 ± 0.00055	30.25	0.0462 ± 0.0006	3.8108 ± 0.0844	52.5 ± 1.2
	05PPT-05b	RN-915	AA-68808	5.00426	0.04249 ± 0.00030	36.61	0.0398 ± 0.0004	3.4132 ± 0.0725	47.0 ± 1.0
	05PPT-05								
	<i>Weighted Mean</i>							<i>3.6038 ± 0.1986</i>	<i>49.7 ± 2.7</i>
	05PPT-08	RN-876	AA-68809	4.99967	0.04086 ± 0.00042	36.24	0.0457 ± 0.0006	3.7605 ± 0.0838	51.8 ± 1.2
	<b>Weighted Mean (n=6)</b>							<b>3.6100 ± 0.0972</b>	<b>49.7 ± 1.3</b>
	<b>Weighted Mean (n=5)</b>								
	<b>(no 05PPT-02)<sup>4</sup></b>							<b>3.7339 ± 0.0539</b>	<b>51.4 ± 0.8</b>

All quoted uncertainties are ± 1σ.

A weighted mean blank value of 2.0750 ± 0.2353 (10<sup>5</sup> <sup>14</sup>C atoms) (n=7) (Appendix A), was used for all <sup>14</sup>C analyses.

Overall site weighted means were calculated using individual analyses and weighted means of replicates.

<sup>1</sup> Uncertainty in measurements is ± 0.0002.

<sup>2</sup> Measured [<sup>14</sup>C] normalized to z = 0 and horizontal surface with no topographic shielding – See Table 1.

<sup>3</sup> Weighted mean of five analyses of one sample and one analysis of a second sample.

<sup>4</sup> Weighted mean excluding sample 05PPT-02.

Table 3. Sample Results and Production Rate Estimates for Northwestern Scotland Sites

Sample Site	Sample	Lab number	AMS number	Mass of quartz analyzed (g) <sup>1</sup>	V <sub>CO<sub>2</sub></sub> (ml)	Dilution Factor	F <sub>m</sub>	Normalized [ <sup>14</sup> C] (10 <sup>5</sup> <sup>14</sup> C atoms/g SiO <sub>2</sub> ) <sup>2</sup>	P <sub>0</sub> at Site ( <sup>14</sup> C atoms/g SiO <sub>2</sub> )/y	
NW SCOTLAND										
Corrie nan Arr	06HKY-01	RN-886	AA-78111	4.99727	0.03631 ± 0.00026	39.33	0.0189 ± 0.0006	1.1645 ± 0.0759	18.7 ± 1.2	
	06HKY-03	RN-899	AA-78113	4.99797	0.03242 ± 0.00028	40.83	0.0191 ± 0.0004	1.1002 ± 0.0644	17.6 ± 1.0	
	06HKY-04	RN-856	AA-78114	5.00538	0.04123 ± 0.00046	35.39	0.0173 ± 0.0003	1.2228 ± 0.0414	19.6 ± 0.7	
<b>Weighted Mean (n=3)</b>								<b>1.1874 ± 0.0350</b>	<b>19.0 ± 0.6</b>	
Maol-Chean-dearg	06HKY-05a	RN-857	AA-78115	5.00524	0.05155 ± 0.00057	28.33	0.0226 ± 0.0004	1.6985 ± 0.0498	27.2 ± 0.8	
	06HKY-05b	RN-897	AA-78115	5.00276	0.04222 ± 0.00033	31.77	0.0232 ± 0.0004	1.4559 ± 0.0640	23.4 ± 1.0	
	06HKY-05c	RN-914	AA-78115	5.00303	0.04576 ± 0.00031	34.53	0.0178 ± 0.0002	1.2506 ± 0.0576	20.1 ± 0.9	
	<i>06HKY-05 Weighted Mean</i>								<i>1.5424 ± 0.1296</i>	<i>24.7 ± 2.1</i>
	06HKY-06a	RN-888	AA-78116	5.00183	0.04387 ± 0.00065	32.40	0.0258 ± 0.0006	1.8330 ± 0.0788	29.4 ± 1.3	
	06HKY-06b	RN-913	AA-78116	5.00270	0.04693 ± 0.00032	33.88	0.0188 ± 0.0006	1.3795 ± 0.0832	22.1 ± 1.3	
	<i>06HKY-06 Weighted Mean</i>								<i>1.6802 ± 0.2144</i>	<i>26.9 ± 3.4</i>
	06HKY-07	RN-890	AA-78117	4.99894	0.03732 ± 0.00031	37.39	0.0226 ± 0.0004	1.5053 ± 0.0660	24.1 ± 1.1	
	06HKY-08	RN-892	AA-78118	5.00390	0.03668 ± 0.00024	37.63	0.0230 ± 0.0004	1.4905 ± 0.0645	23.9 ± 1.0	
	06HKY-09	RN-901	AA-78119	5.00484	0.03225 ± 0.00021	40.64	0.0234 ± 0.0004	1.4468 ± 0.0643	23.2 ± 1.0	
	06HKY-10	RN-906	AA-78120	5.00203	0.04292 ± 0.00033	29.74	0.0249 ± 0.0004	1.5273 ± 0.0641	24.5 ± 1.0	
06HKY-11	RN-908	AA-78121	4.99864	0.03905 ± 0.00024	32.29	0.0264 ± 0.0004	1.6235 ± 0.0639	26.0 ± 1.0		
<b>Weighted Mean (n=7)</b>								<b>1.5280 ± 0.0280</b>	<b>24.5 ± 0.5</b>	

## Notes:

All quoted uncertainties are ± 1σ.

A weighted mean blank value of 1.4658 ± 0.0836 (10<sup>5</sup> <sup>14</sup>C atoms) (n=11) (Appendix A), was used for <sup>14</sup>C calculations for samples 06HKY-04 and 06HKY-05a. A weighted mean blank value of 2.0750 ± 0.2353 (10<sup>5</sup> <sup>14</sup>C atoms) (n=7) (Appendix A), was used for all other <sup>14</sup>C analyses.

Overall site weighted means were calculated using individual analyses and weighted means of replicates.

<sup>1</sup> Uncertainty in measurements is ± 0.0002.

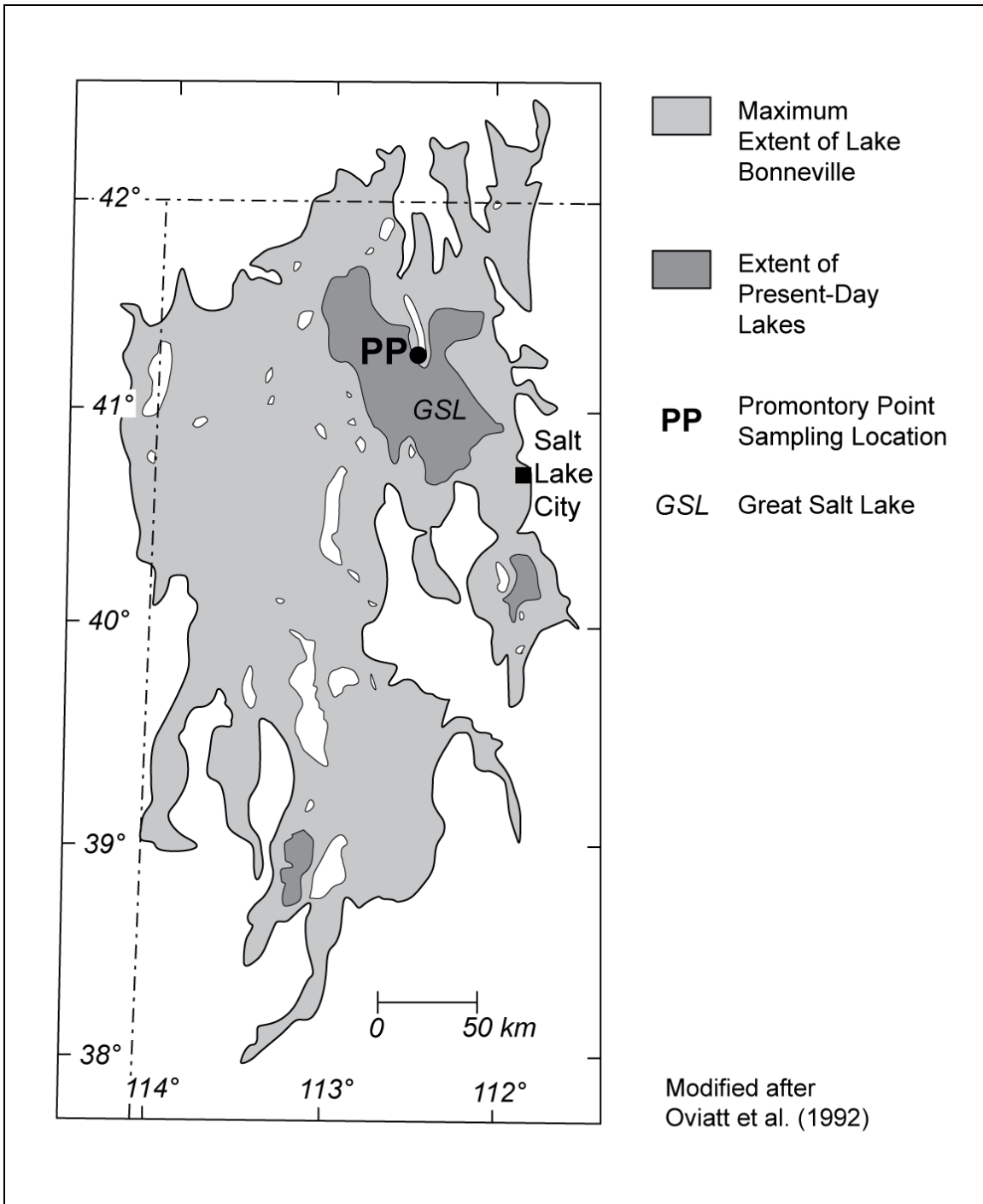
<sup>2</sup> Measured [<sup>14</sup>C] normalized to z = 0 and horizontal surface with no topographic shielding – See Table 1.

Table 4. In Situ  $^{14}\text{C}$  Production Rate Estimates at Sea Level and High Latitude

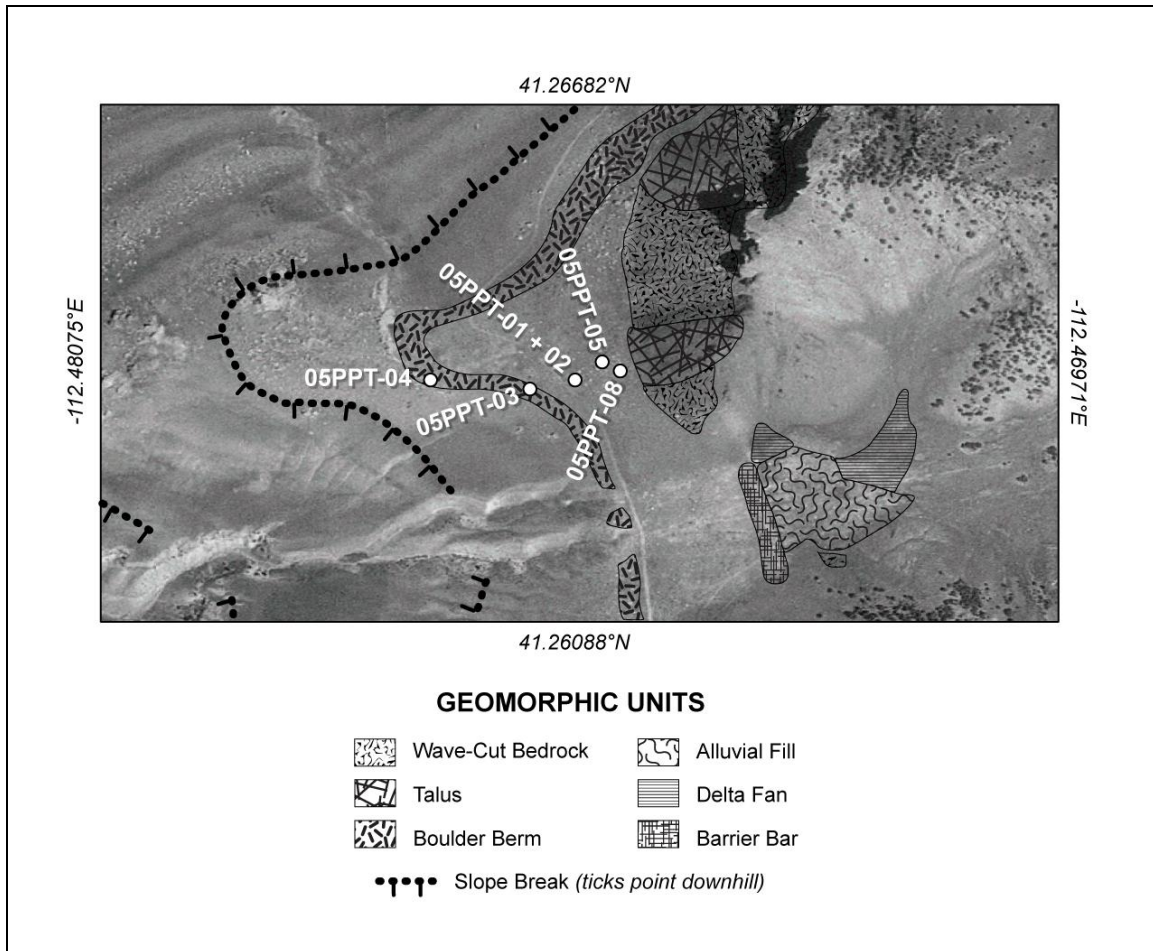
Sample ID	Lal(1991)/ Stone(2000) <sup>1</sup>	Lal (1991)/Stone (2000), geomag <sup>2</sup>	Dunai (2001) <sup>2</sup>	Desilets and Zreda (2006) <sup>2</sup>	Lifton et al. (2005) <sup>2</sup>
<b>LAKE BONNEVILLE</b>					
<i>Lifton et al. (2001)</i>					
<b>Weighted Mean (n=6)</b>	<b>16.67 ± 0.59</b>	<b>16.20 ± 0.57</b>	<b>17.48 ± 0.61</b>	<b>17.24 ± 0.61</b>	<b>19.22 ± 0.67</b>
<i>Miller et al. (2006)</i>					
<b>Weighted Mean (n=10)</b>	<b>15.53 ± 0.22</b>	<b>15.09 ± 0.22</b>	<b>16.29 ± 0.23</b>	<b>16.07 ± 0.23</b>	<b>17.91 ± 0.26</b>
<i>This Study</i>					
05PPT-01	16.63 ± 0.37	16.16 ± 0.36	17.44 ± 0.39	17.20 ± 0.38	19.17 ± 0.43
05PPT-03	16.24 ± 0.36	15.77 ± 0.35	17.03 ± 0.38	16.79 ± 0.37	18.72 ± 0.42
05PPT-04 (Weighted Mean)	14.87 ± 0.64	14.44 ± 0.63	15.60 ± 0.68	15.38 ± 0.67	17.14 ± 0.74
05PPT-05 (Weighted Mean)	15.66 ± 0.86	15.21 ± 0.84	16.42 ± 0.90	16.20 ± 0.89	18.05 ± 0.99
05PPT-08	16.33 ± 0.36	15.86 ± 0.35	17.12 ± 0.38	16.88 ± 0.38	18.82 ± 0.42
<b>Weighted Mean (n=5)</b>	<b>16.25 ± 0.23</b>	<b>15.78 ± 0.22</b>	<b>17.04 ± 0.24</b>	<b>16.80 ± 0.24</b>	<b>18.73 ± 0.26</b>
<b>NW SCOTLAND</b>					
<i>Corrie nan Arr</i>					
06HKY-01	15.96 ± 1.04	15.96 ± 1.04	16.69 ± 1.09	16.36 ± 1.07	17.51 ± 1.15
06HKY-03	15.12 ± 0.88	15.12 ± 0.89	15.81 ± 0.93	15.50 ± 0.91	16.59 ± 0.98
06HKY-04	16.71 ± 0.56	16.71 ± 0.56	17.47 ± 0.60	17.13 ± 0.57	18.34 ± 0.63
<b>Weighted Mean (n=3)</b>	<b>16.25 ± 0.45</b>	<b>16.26 ± 0.45</b>	<b>16.99 ± 0.48</b>	<b>16.67 ± 0.47</b>	<b>17.83 ± 0.50</b>
<i>Maol Chean-dearg</i>					
06HKY-05 (Weighted Mean)	14.77 ± 0.42	14.76 ± 0.42	15.68 ± 0.30	15.38 ± 0.28	16.68 ± 0.32
06HKY-06 (Weighted Mean)	16.16 ± 2.06	16.15 ± 2.06	17.16 ± 2.19	16.83 ± 2.15	18.25 ± 2.33
06HKY-07	14.82 ± 0.65	14.81 ± 0.65	15.73 ± 0.69	15.43 ± 0.68	16.72 ± 0.74
06HKY-08	14.65 ± 0.63	14.64 ± 0.63	15.55 ± 0.68	15.25 ± 0.66	16.53 ± 0.72
06HKY-09	14.22 ± 0.63	14.21 ± 0.63	15.09 ± 0.68	14.80 ± 0.66	16.04 ± 0.72
06HKY-10	14.90 ± 0.63	14.89 ± 0.63	15.82 ± 0.67	15.52 ± 0.65	16.83 ± 0.71
06HKY-11	15.60 ± 0.61	15.59 ± 0.61	16.57 ± 0.66	16.25 ± 0.64	17.62 ± 0.70
<b>Weighted Mean (n=7)</b>	<b>14.86 ± 0.23</b>	<b>14.85 ± 0.23</b>	<b>15.75 ± 0.21</b>	<b>15.45 ± 0.20</b>	<b>16.75 ± 0.23</b>
<b>ALL THREE SITES</b>					
<b>Unweighted Mean (n=3) <sup>3</sup></b>	<b>15.79 ± 0.46</b>	<b>15.63 ± 0.41</b>	<b>16.59 ± 0.42</b>	<b>16.31 ± 0.43</b>	<b>17.77 ± 0.57</b>
<i>Percentage uncertainty</i>	± 2.93%	± 2.64%	± 2.53%	± 2.64%	± 3.21%

Notes:

All quoted uncertainties are  $\pm 1\sigma$ .All values are in units of  $^{14}\text{C}$  atoms  $(\text{g SiO}_2)^{-1} \text{y}^{-1}$ .<sup>1</sup> Assumes a GAD geomagnetic model.<sup>2</sup> Assumes the Lifton et al. (2008) geomagnetic framework. Modified for Lal (1991)/Stone (2000) model following Balco et al. (2008).<sup>3</sup>  $\pm$  Standard error.



Dugan et al.  
FIGURE 1



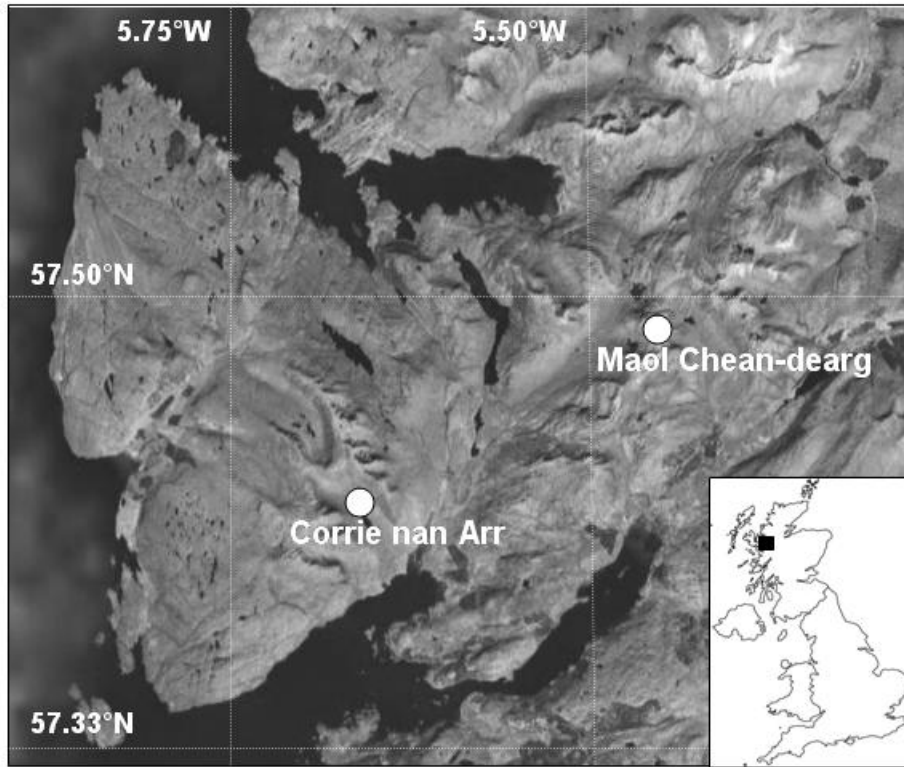
Dugan et al.  
FIGURE 2



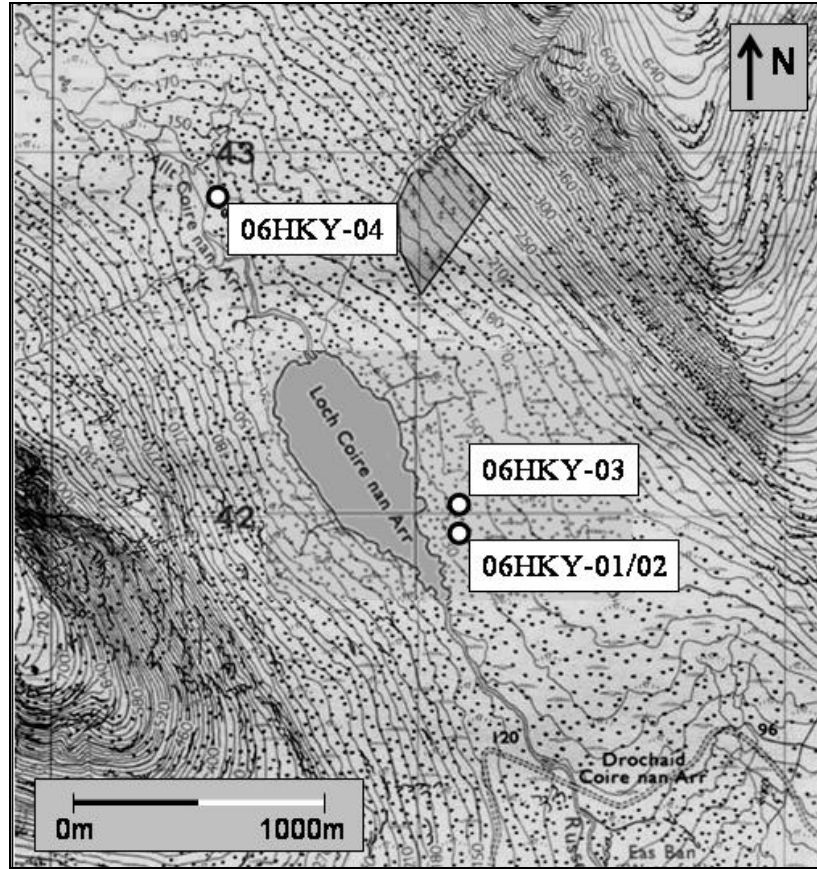
Dugan et al.  
FIGURE 3



Dugan et al.  
FIGURE 4



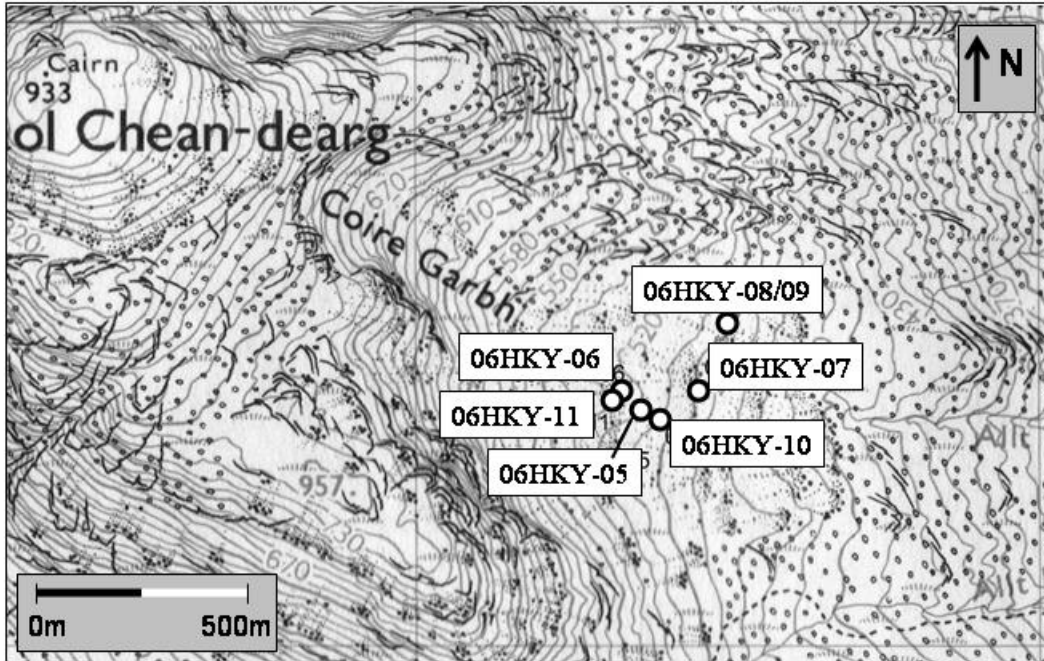
Dugan et al.  
FIGURE 5



Dugan et al.  
FIGURE 6A



Dugan et al.  
FIGURE 6B



Dugan et al.  
FIGURE 7A



Dugan et al.  
FIGURE 7B

## APPENDIX A

Table A1. Blank data used in calculations

Extraction System	Lab Number	AMS Number	$V_{CO_2}$ (ml)	Dilution Factor	$F_m$	$N_{14}$ ( $10^5$ atoms) <sup>1</sup>
Flow-through System	RN-841	AA-77292	$0.01264 \pm 0.00233$	91.53	$0.0071 \pm 0.0002$	$2.0347 \pm 0.0967$
	RN-848	AA-77292	$0.01403 \pm 0.00234$	87.52	$0.0076 \pm 0.0003$	$2.3778 \pm 0.1350$
	RN-858	AA-77292	$0.01306 \pm 0.00235$	92.04	$0.0050 \pm 0.0002$	$1.3188 \pm 0.1000$
	RN-875	AA-77292	$0.02066 \pm 0.00237$	71.70	$0.0073 \pm 0.0003$	$2.7952 \pm 0.1621$
	RN-879	AA-77292	$0.01267 \pm 0.00233$	115.78	$0.0069 \pm 0.0004$	$2.5783 \pm 0.2031$
	RN-902	AA-77292	$0.00956 \pm 0.00235$	133.21	$0.0052 \pm 0.0002$	$1.4981 \pm 0.1055$
	RN-910	AA-77292	$0.01051 \pm 0.00234$	116.01	$0.0034 \pm 0.0001$	$0.7163 \pm 0.0751$
	<b>Weighted Mean</b>					
Recirculating System	RN-632	AA-41990	$0.00762 \pm 0.00007$	165.69	$0.0039 \pm 0.0003$	$0.9446 \pm 0.1386$
	RN-635	AA-41990	$0.00970 \pm 0.00074$	125.89	$0.0048 \pm 0.0003$	$1.2539 \pm 0.1344$
	RN-636	AA-41990	$0.01163 \pm 0.00080$	103.81	$0.0064 \pm 0.0003$	$1.8546 \pm 0.1336$
	RN-647	AA-41990	$0.01082 \pm 0.00044$	98.98	$0.0052 \pm 0.0005$	$1.1937 \pm 0.1814$
	RN-649	AA-41990	$0.00998 \pm 0.00026$	136.18	$0.0048 \pm 0.0002$	$1.4474 \pm 0.1129$
	RN-650	AA-41990	$0.01225 \pm 0.00092$	88.88	$0.0063 \pm 0.0003$	$1.6033 \pm 0.1209$
	RN-709	AA-41990	$0.00683 \pm 0.00103$	193.69	$0.0035 \pm 0.0002$	$0.8387 \pm 0.110$
	RN-746	AA-58401	$0.00796 \pm 0.00049$	154.84	$0.0055 \pm 0.0002$	$1.5466 \pm 0.1034$
	RN-747	AA-58401	$0.00977 \pm 0.00144$	206.33	$0.0022 \pm 0.0002$	$0.6222 \pm 0.1645$
	RN-831	AA-58401	$0.01158 \pm 0.00089$	112.02	$0.0050 \pm 0.0004$	$1.5293 \pm 0.1790$
	RN-843	AA-58401	$0.01073 \pm 0.00046$	115.61	$0.0048 \pm 0.0003$	$1.2921 \pm 0.1360$
	<b>Weighted Mean</b>					

Notes:

All quoted uncertainties are  $\pm 1\sigma$ .

All samples were run on the flow-through system except samples 06HKY-04 and 06HKY-05a, which were run on the recirculating system

<sup>1</sup> Number of <sup>14</sup>C atoms from Equation (4), with B=0 and M=1.